Chem. Mater. **1996,** *8,* 2421−2432

Reviews

Giant Magnetoresistance and Related Properties of Rare-Earth Manganates and Other Oxide Systems

C. N. R. Rao,*,[†,‡] A. K. Cheetham,*,[†] and R. Mahesh[‡]

Materials Research Laboratory, University of California, Santa Barbara, California 93106, and Solid State and Structural Chemistry Unit, Indian Institute of Science, Bangalore 560 012, India

Received March 26, 1996. Revised Manuscript Received June 20, 1996[⊗]

Giant magnetoresistance (GMR), which was until recently confined to magnetic layered and granular materials, as well as doped magnetic semiconductors, occurs in manganate perovskites of the general formula $Ln_{1-x}A_xMnO_3$ (Ln = rare earth; A = divalent ion). These manganates are ferromagnetic at or above a certain value of x (or Mn^{4+} content) and become metallic at temperatures below the curie temperature, T_c. GMR is generally a maximum close to T_c or the insulator−metal (I−M) transition temperature, T_{im}. The T_c and %MR are markedly affected by the size of the A site cation, $\langle r_A \rangle$, thereby affording a useful electronic phase diagram when T_c or T_{im} is plotted against $\langle r_A \rangle$. We discuss GMR and related properties of manganates in polycrystalline, thin-film, and single-crystal forms and point out certain commonalities and correlations. We also examine some unusual features in the electron-transport properties of manganates, in particular charge-ordering effects. Charge ordering is crucially dependent on $\langle r_A \rangle$ or the e_g band width, and the charge-ordered insulating state transforms to a metallic ferromagnetic state on the application of a magnetic field.

Introduction

Magnetoresistance (MR) is the change in the electrical resistance of a material produced on applying a magnetic field, H. MR is generally defined by the equation

$$MR = [\Delta\rho/\rho(0)] = [\rho(H) - \rho(0)]/\rho(0) \quad (1)$$

where $\rho(H)$ and $\rho(0)$ are the resistances at a given temperature in the applied and zero magnetic fields, respectively. MR can be negative or positive. All metals show some MR, but only a few percent. Nonmagnetic metals, such as Au, exhibit small MR, but the magnitude is somewhat greater (up to 15%) in ferromagnetic metals such as Fe and Co. Very large magnetoresistance, referred to as giant magnetoresistance (GMR), was first observed on the application of magnetic fields to atomically engineered magnetic superlattices (e.g., Fe/Cr).[1,2] Several bimetallic or multimetallic layers, containing ferromagnetic and antiferromagnetic or nonmagnetic metals, have since been found to exhibit GMR. Besides magnetic layered materials, GMR has been found in ferromagnetic granules dispersed in paramagnetic metal films (e.g., Co/Cu).[3] GMR in magnetic multilayer and granular materials has been investigated by a wide range of methods in the past few years.[4] The phenomenon is of vital interest because of its potential technological applications in magnetic recording, actuators, and sensors.

GMR in magnetic layered and granular materials arises from the ability of magnetic fields to change and control the scattering of conduction electrons in metals through the modification of the electron−orbit and spin−orbit interactions. It is believed to be essentially a manifestation of spin-dependent scattering. The applied magnetic field reorients the ferromagnetic components to an aligned state, generating a magnetic disorder−order transition. GMR is then the extra resistance due to the scattering of electrons by the nonaligned ferromagnetic components in zero magnetic field. There has been considerable effort to understand the origin of GMR in magnetic multilayers,[4] but there are yet some unresolved issues such as the effect of the band structure of the magnetic multilayers on the transport properties. Besides magnetic layered and granular materials, GMR has been observed in doped magnetic semiconductors, such as n-$Cd_{1-x}Mn_xSe$.[5] In these materials, GMR is maximum when the carrier concentration is in the critical region across the metal−insulator boundary.

The recent discovery of GMR in rare-earth manganates,[6−9] $Ln_{1-x}A_xMnO_3$ (Ln = rare earth, A = a divalent cation such as Ca, Sr, Ba, Pb) with the perovskite structure has attracted considerable attention, not only because these oxides are new GMR systems but also because they exhibit several novel features. In the past three years, a variety of manganates have been investigated in the form of polycrystalline powders, thin films, and single crystals. These studies have provided a wealth of information on the GMR phenomena in metal oxides, as well as on the nature of the oxides themselves. In what follows, we present the highlights of the findings on the GMR and related properties of the manganates and related sys-

[†] University of California, Santa Barbara.
[‡] Indian Institute of Science, Bangalore.
[⊗] Abstract published in *Advance ACS Abstracts,* September 15, 1996.

S0897-4756(96)00201-3 CCC: $12.00

tems with emphasis on material aspects. We point out important generalizations with regard to the dependence of the properties on the composition, structure, and other factors and also examine the interrelations between the magnetic and electron-transport properties. We also discuss certain unusual and interesting aspects of the manganates; in particular, charge ordering effects seen abundantly in these oxides. The competition between charge and spin ordering in these systems is clearly a topic of vital interest.

Preliminaries

$LaMnO_3$, as prepared by the solid-state reaction between the oxides and carbonates of the component metals, is an insulating perovskite with an orthorhombic structure ($b > a > c^{1/2}$, *Pbnm*) and typically contains around 10% Mn^{4+}. $LaMnO_3$ with a small proportion of Mn^{4+} (<5%) becomes antiferromagnetically ordered below $T_N = 150$ K. The $La_{1-x}A_xMnO_3$ system (A = Ca, Sr, or Ba), where the La^{3+} in $LaMnO_3$ is progressively substituted by a divalent cation, was investigated several years ago by Jonker and van Santen,[10] who found an empirical relationship between electrical conduction and magnetism in these materials. With increase in x (or the Mn^{4+} content), the manganates became ferromagnetic with well-defined Curie temperatures, T_c. Around T_c, they also exhibited metal-like conductivity. The simultaneous observation of itinerant electron behavior and ferromagnetism in the manganates is explained by the double-exchange mechanism, due to Zener.[11] The basic process in this mechanism is the hopping of a d hole from Mn^{4+} (d^3, $t_{2g}{}^3$, $S = {}^3/_2$) to Mn^{3+} (d^4, $t_{2g}{}^3$ $e_g{}^1$, $S = 2$) via the oxygen, so that the Mn^{4+} and Mn^{3+} ions change places. According to this mechanism, a paramagnetic to ferromagnetic transition should occur, as described by

$$k_B T_c \sim x_h \xi t \qquad (2)$$

where x_h is the hole concentration (Mn^{4+}), t is the hole-hopping amplitude, and ξ is the number of nearest neighbors. Electronically, the system is expected to be a disordered metal (or insulator) in the paramagnetic phase with the holes diffusing through a collection of fluctuating spins, and a metal in the ferromagnetic phase whose resistivity decreases as the magnetization increases below T_c. The $t_{2g}{}^3$ electrons of the Mn^{3+} ion are localized on the Mn site giving rise to a local spin of ${}^3/_2$, but the e_g state, which is hybridized with the oxygen 2p state, can be localized or itinerant. There is strong interaction between the e_g electron and the $t_{2g}{}^3$ spins. Goodenough[12] suggested that ferromagnetism is governed not only by double exchange but also by the nature of the superexchange interactions. de Gennes[13] clearly delineated the nature of the double-exchange interaction (as distinct from the exchange interaction) and pointed out that a noncollinear magnetic structure forms at intermediate concentrations between the antiferromagnetic and the ferromagnetic states. It may be recalled that the Mn^{3+}–O–Mn^{4+} exchange interaction is ferromagnetic while the Mn^{3+}–O–Mn^{3+} and Mn^{4+}–O–Mn^{4+} interactions are antiferromagnetic.

$LaMnO_3$ and $AMnO_3$, the $x = 0.0$ and the $x = 1.0$ members of the $La_{1-x}A_xMnO_3$ system, are AFM insulators at low temperatures, with A- and G-type ordering,

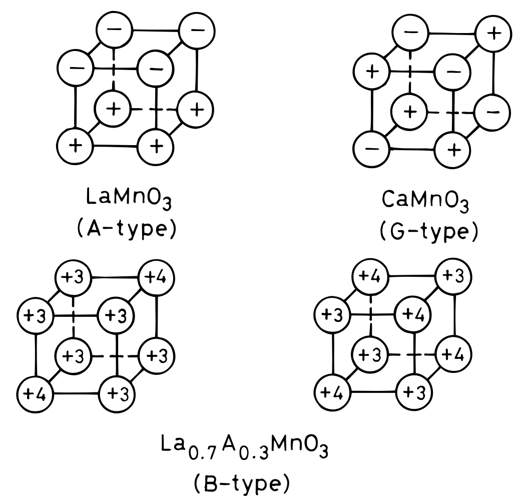

Figure 1. Magnetic structure of antiferromagnetic $LaMnO_3$, antiferromagnetic $CaMnO_3$, and ferromagnetic $La_{0.7}A_{0.3}MnO_3$. Two possible FM orderings of Mn ions are shown for the latter (after ref 14).

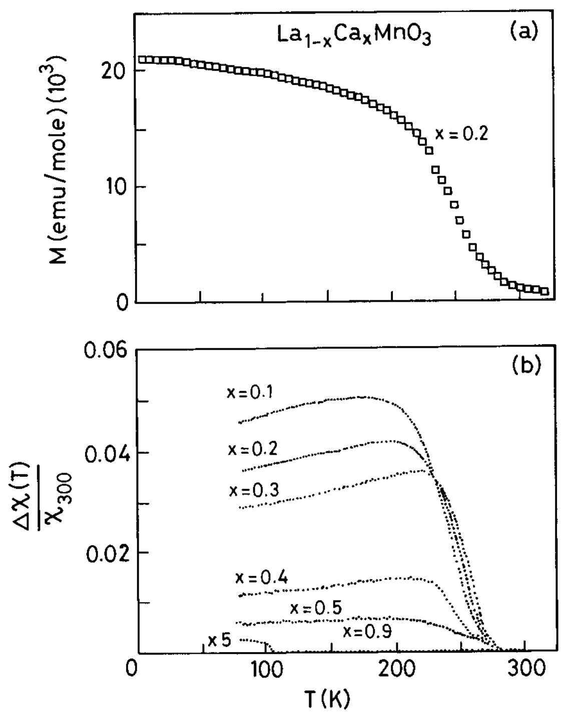

Figure 2. Magnetization and ac magnetic susceptibility of $La_{1-x}A_xMnO_3$ compositions (after ref 15).

respectively[14] (see Figure 1). Ferromagnetic behavior starts to manifest itself when x is ~0.1, and the compositions up to $x \sim 0.3$ have both AFM and FM characteristics.[14] The $x = 0.3$ composition is purely ferromagnetic, while the $x > 0.5$ compositions are antiferromagnetic. In Figure 1, we show the antiferromagnetic ordering in $LaMnO_3$ and the ferromagnetic ordering in $La_{0.7}Ca_{0.3}MnO_3$. The FM transitions in the $La_{1-x}A_xMnO_3$ compositions are quite sharp,[15] as can be seen from Figure 2. Although manganates with $x > 0.5$ are essentially antiferromagnetic, there would be FM Mn^{3+}–O–Mn^{4+} clusters in the AFM medium. Figure 3 illustrates how the magnetic properties of $La_{1-x}Ca_xMnO_3$ change with the compositions.[16]

It was mentioned above that as-prepared $LaMnO_3$ contains around 10% Mn^{4+}. The origin of Mn^{4+} has been examined in some detail. Since perovskites cannot

Table 1. Properties of $Ln_{1-x}A_xMnO_3$

composition	Mn^{4+} [a] (%)	structure	lattice parameters	form [b] of the sample	T_{im} (K)	T_c (K)	ρ_p (Ω cm)	MR [c] (%)	ref
$LaMnO_3$	24	rhombohedral	$a = 5.478$ Å, $\alpha = 60.55°$	PC	180	230	11.5	53 (6 T)	15
	33	cubic	$a = 7.788$ Å	PC	200	240	3	68 (6 T)	15
$La_{0.7}Ca_{0.3}MnO_3$	33	pseudocubic	$a = 7.699$ Å	PC	260	260	0.2	55 (6 T)	15
				TF	250	250	0.018	85 (5 T)	32(f)
$La_{0.7}Sr_{0.3}MnO_3$	37	rhombohedral	$a = 5.454$ Å, $\alpha = 60.14°$	PC	330	360	0.016	45 (6 T)	15
				TF	370	369	0.008	35 (5 T)	9
	28	rhombohedral		SC	370	310	0.014		32(c)
$La_{0.67}Ba_{0.33}MnO_3$	31	pseudocubic	a = 7.794 Å	PC	340	340	0.012	40 (5 T)	44
		rhombohedral	$a = 5.529$ Å, $\alpha = 60.08°$	TF	300	340	0.008	60 (5 T)	6(a)
$Nd_{0.7}Sr_{0.3}MnO_3$	28	pseudocubic	$a = 7.738$ Å	PC	185	195	5	54 (6 T)	27
				TF	60		265	99.99 (8 T)	39

[a] Obtained by redox titrations. [b] PC, polycrystal; SC, single crystal; TF, thin film. [c] Magnetic field strength is shown in parentheses.

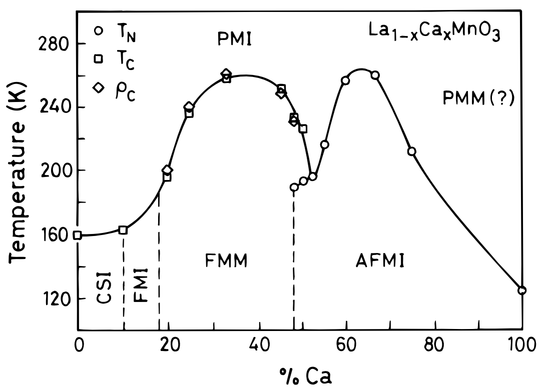

Figure 3. Approximate temperature−composition diagram of $La_{1-x}A_xMnO_3$: CSI, canted-spin insulator; FMI, ferromagnetic insulator; FMM, ferromagnetic metal; AFMI, antiferromagnetic insulator; PMI, paramagnetic insulator; PMM, paramagnetic metal (adapted from ref 16).

accommodate excess oxygen, the defect chemistry of $LaMnO_3$ must involve the presence of cation vacancies in the La and Mn sites.[17] Accordingly, $LaMnO_3$ is considered to be $La_{1-\delta}Mn_{1-\delta}O_3$. If the Mn^{4+} content in $LaMnO_3$ is 33%, the formula will approximately correspond to $La_{0.945}Mn_{0.945}O_3$. It is to be noted that the parent $LaMnO_3$ becomes rhombohedral and then cubic as the Mn^{4+} content is increased by chemical or electrochemical means.[18] Nominal $La_{1-\delta}MnO_3$ and $LaMn_{1-\delta'}O_3$ compositions have been prepared. The $La_{1-\delta}MnO_3$ compositions exhibit ferromagnetism and the I−M transition up to $\delta = 0.3$, but $LaMn_{1-\delta'}O_3$ compositions do so only up to $\delta' = 0.05$.[18]

The structural chemistry for $La_{1-x}A_xMnO_3$ is also based on this model for the parent manganate. The orthorhombic distortion in $LaMnO_3$ decreases as La is progressively substituted by a divalent ion, and the material becomes essentially pseudocubic at some value of x. The structures of $La_{1-x}A_xMnO_3$ compositions are therefore described as orthorhombic (*Pbnm*), rhombohedral ($R\bar{3}c$), or pseudocubic. The same is broadly true for other rare-earth manganates, $Ln_{1-x}A_xMnO_3$ (Ln = Pr, Nd, etc.). We list the unit-cell parameters of a few typical compositions in Table 1. The transfer interaction of e_g electrons is greater in the rhombohedral or pseudocubic phase than in the orthorhombic phase. The compositions with high symmetry structures (e.g., pseudocubic), as determined by ordinary powder X-ray diffraction, may turn out to be of lower symmetry (e.g., orthorhombic) when examined with synchrotron radiation or neutron diffraction.

Cation size also plays an important role in manganates of the type $Ln_{1-x}A_xMnO_3$ (Ln = La, Pr, Y; A = Ca, Sr, Ba); the structure is orthorhombic when the average size of the A-site cations, $\langle r_A \rangle$, is small (<1.23). With increase in $\langle r_A \rangle$, the structure becomes rhombohedral down to very low temperatures. However, in $La_{0.7}Ba_{0.3}MnO_3$ a new orthorhombic structure (*Imma*) has been observed below 150 K, the $R\bar{3}c \rightarrow Imma$ transition being first order.[19] In $La_{1-x}Sr_xMnO_3$ ($x \sim 0.17$), two insulating orthorhombic states have been identified by Yoshizawa[20] with a phase boundary at $x = 0.1$. Yamada[20] has found polaron ordering at such doping.

X-ray crystallographic studies of $LaMnO_3$ suggest that the removal of the static Jahn−Teller distortion is a first order transition.[21a] In $La_{0.5}Ca_{0.5}MnO_3$, a drastic decrease in the *b* parameter and an increase in the *a* and *c* parameters are found due to the Jahn−Teller (J−T) distortions of the MnO_6 octahedra below 225 K.[21b] Raveau and co-workers[21c] have observed variations in the *a*, *b*, and *c* parameters of $Pr_{0.7}Ca_{0.2}Sr_{0.1}MnO_3$ and an increase in one of the Mn−O distances by 0.01 Å due to J−T distortion at T_c. Such changes, along with those associated with the ordering of valence states, are indeed of considerable interest and are discussed in a later section.

Electron-Transport Properties and GMR

$La_{1-x}A_xMnO_3$ compositions are generally insulators at ordinary temperatures (say, 300 K or higher) and exhibit an increase in electrical resistivity with a decrease in temperature. Compositions that are ferromagnetic show insulating behavior above T_c, but the resistivity decreases with decreasing temperature, as in metals, when they are cooled below T_c. This insulator−metal transition (I−M) is therefore associated with a peak in resistivity at a temperature T_{im}. In Figure 4 we show typical I−M transitions in polycrystalline $La_{1-x}Ca_xMnO_3$ samples. Such a transition is also exhibited by $LaMnO_3$ with a sufficient proportion of Mn^{4+}. T_{im} is always lower than T_c. We list the T_{im} and T_c values in a few polycrystalline manganates in Table 1.

Since the presence of an adequate proportion of Mn^{4+} is essential for the ferromagnetism and the consequent I−M transition, it is desirable to independently determine the Mn^{4+} content by means of redox titrations (Fe(II) sulfate + $KMnO_4$). It can be somewhat misleading to assume that the Mn^{4+} content is simply dictated by

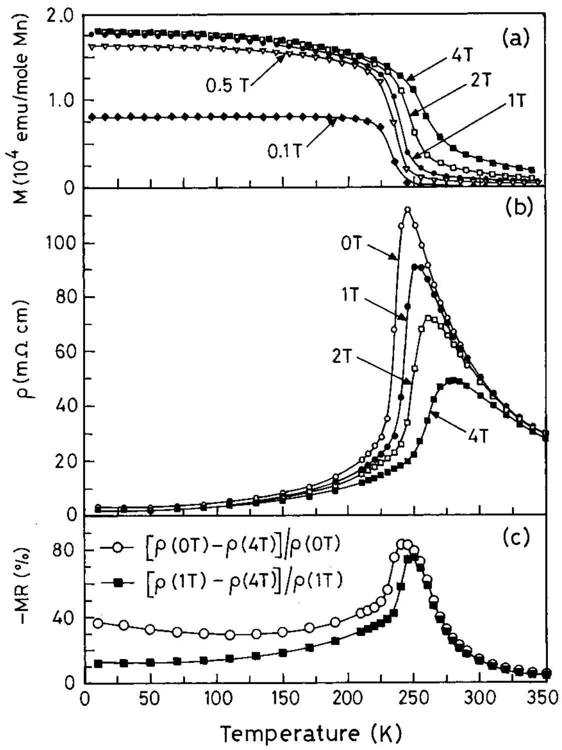

Figure 4. Temperature variation of magnetization, resistivity and magnetoresistance of $La_{0.75}Ca_{0.25}MnO_3$ in various fields (from ref 16).

the formula $La_{1-x}A_xMnO_3$, since it can vary with the method of preparation (e.g., solid-state reaction at high temperatures vs low-temperature sol−gel method) and the heating schedule employed. In Table 1 we list the Mn^{4+} content in a few polycrystalline samples, as determined by redox titrations.

The application of a magnetic field (up to, say, 6 T) causes a significant decrease in the resistivity of the $La_{1-x}A_xMnO_3$ samples, particularly in the compositions with $0.1 < x < 0.5$; these materials are generally ferromagnetic with well-defined T_c's. The magnitude of the decrease in resistivity (i.e., the magnetoresistance, MR) is highest in the region of T_c or T_{im}. In Figure 4 we compare the temperature variation of the resistivity of $La_{1-x}Ca_xMnO_3$ at 4 T with that in zero field. Magnetoresistance in the manganates is generally negative. In Figure 5 we show the variation in %MR with temperature in polycrystalline $La_{1-x}Ca_xMnO_3$. We see that the %MR varies from one composition to another and can be very high,[22] especially in the region of T_c; some compositions show a peak in MR at a temperature close to T_{im}. GMR close to 100% has been observed in many polycrystalline $La_{1-x}A_xMnO_3$ compositions (e.g., at 300 K and higher for A = Pb), but the applied field is always quite high (5−6 T).[23] The variation of %MR with field is shown in Figure 6. We notice a sharp decrease in the MR at low fields (<1 T), followed by a gradual change. The %MR−H variation parallels the variation in magnetization with H, the initial change at small H being associated with magnetic domain growth. Self-doped $LaMnO_3$ samples with increased Mn^{4+} content (i.e., $La_{1-\delta}Mn_{1-\delta}O_3$) exhibit GMR similar to that observed in the $La_{1-x}A_xMnO_3$ compositions;[15] in Figure 7 we show the behavior of $La_{0.945}Mn_{0.945}O_3$, with 33% Mn^{4+}. La-deficient $La_{1-\delta}MnO_3$ compositions also exhibit GMR, but Mn-deficient $LaMn_{1-\delta'}O_3$ samples do not when $\delta' > 0.05$.[18,24]

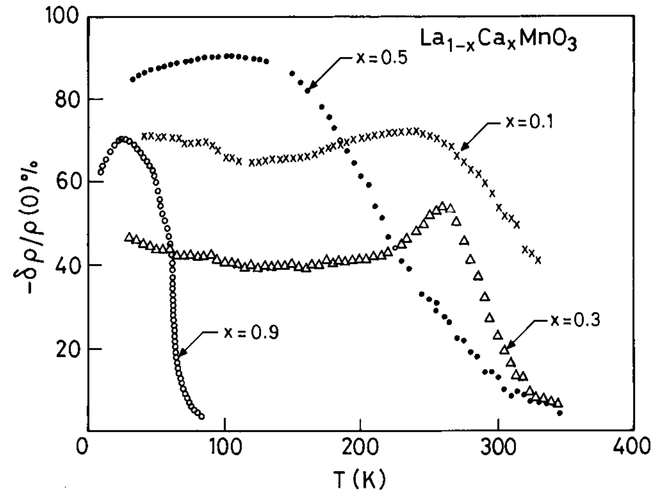

Figure 5. Temperature variation of the magnetoresistance of polycrystalline $La_{1-x}Ca_xMnO_3$.

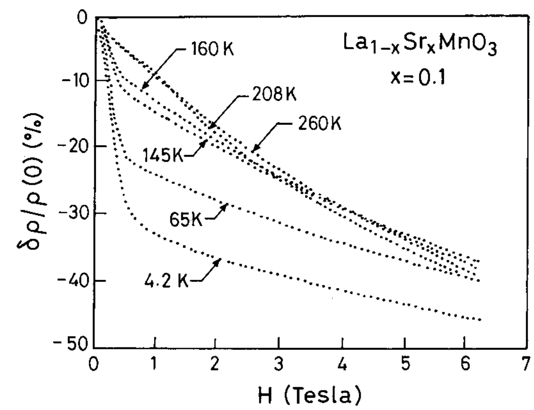

Figure 6. Variation of magnetoresistance of polycrystalline $La_{1-x}Sr_xMnO_3$ with magnetic field, H (from ref 15).

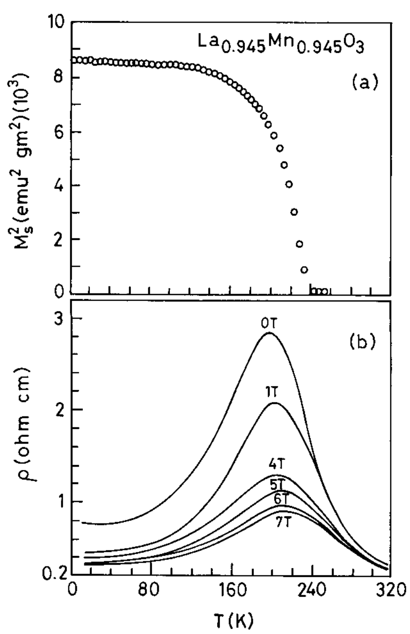

Figure 7. (a) Magnetization data of polycrystalline $La_{0.945}Mn_{0.945}O_3$; (b) resistivity−temperature plots for polycrystalline $La_{0.945}Mn_{0.945}O_3$ at different magnetic fields (after ref 15).

Besides polycrystalline $La_{1-x}A_xMnO_3$ (A = Ca, Sr, Ba) compositions, other rare-earth manganates, $Ln_{1-x}A_xMnO_3$ with Ln = Pr, Nd, Sm, and Gd, have been examined for GMR properties.[25−27] The ferromagnetic T_c's and related properties of these compounds depend on the sizes

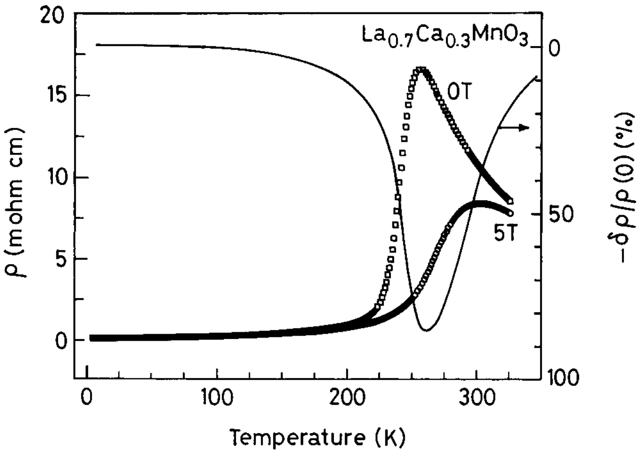

Figure 8. Magnetoresistance of a thin film of $La_{1-x}Ca_xMnO_3$ (after ref 32f).

of the rare-earth and alkaline-earth ions. Generally, T_c decreases with a decrease in the cation size, but the magnitude of the MR is enhanced, as is clearly demonstrated by the yttrium-substituted derivatives.[28,29] Polycrystalline $La_{1-x}Pb_xMnO_3$ exhibits large GMR at room temperature or above.[30] GMR in $(La_{0.75}Tb_{0.25})_{0.67}Ca_{0.33}MnO_3$ is accompanied by magnetovolume effects above T_c; these disappear below T_c, suggesting two different GMR mechanisms above and below T_c.[31]

The electron transport of thin films of $La_{1-x}A_xMnO_3$ is not different from those of the polycrystalline samples discussed hitherto. After the initial reports[8−10] of GMR in thin films of $La_{1-x}A_xMnO_3$ (A = Ca, Sr, Ba), there have been several investigations of thin films of these materials.[32] In Figure 8, we show the resistivity behavior of a typical thin-film preparation in the absence and presence of a magnetic field. Thin films of $Nd_{1-x}Sr_xMnO_3$,[33] $La_{0.6}Y_{0.07}Ca_{0.33}MnO_3$,[34] and $La_{0.6}Pb_{0.4}MnO_3$[35] have been shown to exhibit GMR, as do films of La-deficient $LaMnO_3$.[36] Films of $La_{1-x}Ca_xMnO_3$ show strong Faraday rotation in the vicinity of the 2p(O) → 3d(Mn) charge-transfer adsorption (3 eV), as well as of the $3d(t_{2g}) \rightarrow 3d(e_g)$ excitation (1.5 eV).[37] Magnetoresistance in $La_{0.7}Ca_{0.3}MnO_3$ and $Nd_{0.7}Sr_{0.3}MnO_3$ films shows hysteresis effects, the resistance becoming dependent on magnetic history.[38,39] In the latter case, for example, the film enters a high conductivity state upon application of a magnetic field at temperatures below T_{im}; this persists, even after the field is reduced to zero. Such memory effects have also been observed in polycrystalline samples of $Nd_{1-x}A_xMnO_3$.

GMR studies of single crystals of a few rare-earth manganates have been reported in the literature.[12,40] Although the general features of the transport properties are not very different from those of the polycrystalline samples, there are some subtle differences. For example, the I−M transition does not always show a distinct resistivity peak as in the polycrystalline samples. In Figures 9 and 10, respectively, we show the resistivity behavior (at zero field) and electronic phase diagram of $La_{1-x}Sr_xMnO_3$ crystals. The effect of magnetic field on the resistivity behavior of a typical sample is shown in Figure 11, along with the temperature variation of MR. The reduction in resistivity in these crystals scales with the field-induced magnetization, M, as

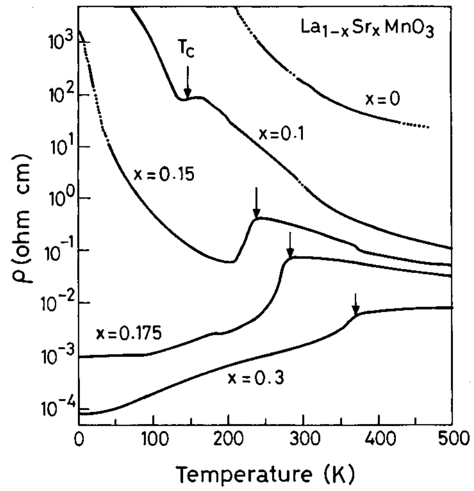

Figure 9. Temperature variation of the resistivity of a single crystal of $La_{1-x}Sr_xMnO_3$ (after ref 9).

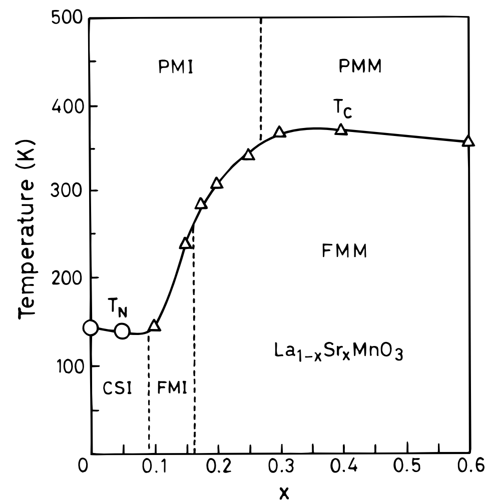

Figure 10. Phase diagram of $La_{1-x}Sr_xMnO_3$ (after ref 9).

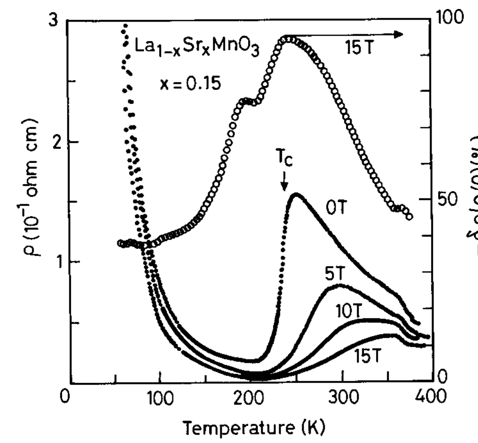

Figure 11. Resistivity−temperature plots of $La_{0.85}Sr_{0.15}MnO_3$ at different magnetic fields (after ref 9).

$$-\Delta\rho/\rho = C(M/M_s)^2 \qquad (3)$$

for $M/M_s < 0.3$, where M_s is the saturation magnetization. MR measurements on single crystals of $La_{0.6}Pb_{0.4}MnO_3$ and $Nd_{0.6}(Sr_{0.7}Pb_{0.3})_{0.4}MnO_3$ show that magnetoresistance vanishes as $T \rightarrow$ zero,[41] unlike in films and polycrystalline materials (see Figures 5, 6, and 8). $La_{0.65}(Pb,Ca)_{0.35}MnO_3$ crystals exhibit a change in the sign of the resistivity−magnetic field curve above and below T_c, indicating two different mechanisms for the

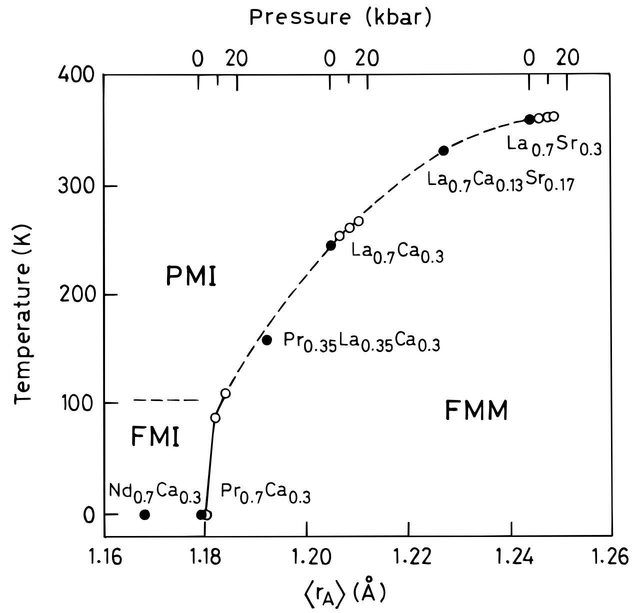

Figure 12. Variation of T_c (T_{im}) of $Ln_{0.7}A_{0.3}MnO_3$ with hydrostatic pressure and the weighted average radius of the A-site cations (from ref 47).

magnetic scattering of carriers in the two temperature regimes.[42]

Commonalities and Correlations

Investigations of the manganates in the past three years enable us to arrive at some generalizations with regard to the major factors responsible for GMR and to correlate the electronic and magnetic properties with structural parameters. In what follows, we present some of the important general features and correlations.

(i) Ferromagnetism in the manganates, and hence the I−M transition and the GMR, are crucially dependent on the Mn^{4+} content.[43] Around 33% Mn^{4+} seems to be optimal, but the compositions with ∼33 ± 5% show similar effects. The resistivity, ρ, also depends upon the Mn^{4+} content, as one would expect. The T_c and ρ are both affected by oxygen stoichiometry,[44] a decrease in the oxygen content increasing ρ and decreasing T_c.

(ii) The insulator-to-metal transition generally occurs just below T_c, and the T_c and T_{im} values are therefore comparable. Maximum GMR also occurs in the T_c, T_{im} region.

(iii) The $Ln_{1-x}A_xMnO_3$ compositions have the orthorhombic structure for small x and tend to become rhombohedral or pseudocubic as x is increased. One would expect maximum GMR when the Mn−O−Mn angle is close to 180°. The Mn−O distance is less than 1.97 Å (optimally ∼ 1.94 Å) in the manganates exhibiting ferromagnetism and GMR.[15]

(iv) Magnetoresistance is high when the T_c or T_{im} is low. High MR is also favored by high resistivity, especially at the I−M transition (ρ_p).

(v) Hydrostatic pressure decreases ρ and increases the T_c markedly[45,46] as can be seen from Figure 12. The increase in T_c with pressure is attributed to changes in the Mn−Mn transfer integral or the Mn−O−Mn angle.

(vi) The T_c value in the manganates is sensitive to the average radius of the A site cations.[25,27,47] By varying the Ln and A ions in $Ln_{1-x}A_xMnO_3$, it has been possible to correlate the T_c with $\langle r_A \rangle$, giving a useful phase diagram that separates the paramagnetic insulator and ferromagnetic metal regimes. The effect of increasing $\langle r_A \rangle$ is equivalent to increasing the pressure. Figure 13, which shows a plot of T_c or T_{im} against $\langle r_A \rangle$ for a large number of perovskites, illustrates the effectiveness of this relation in describing the electronic phase diagram. We notice that at small $\langle r_A \rangle$ we have the ferromagnetic insulator regime. The T_c, T_{im} is highest when the $\langle r_A \rangle$ is 1.23 ± 0.01 Å, which corresponds to a tolerance factor of 0.93. The magnitudes of MR and ρ_p are also sensitive functions of $\langle r_A \rangle$, both decreasing with increasing $\langle r_A \rangle$ (Figure 14). On the basis of these correlations with $\langle r_A \rangle$, we would expect that substitution of yttrium into $La_{1-x}A_xMnO_3$ would markedly affect the MR and related properties. Studies[29,48] have indeed shown the enhancement of MR, the decrease in T_c, and the increase in ρ_p with yttrium substitution. It may be noted that with increase in $\langle r_A \rangle$, the e_g bandwidth increases.

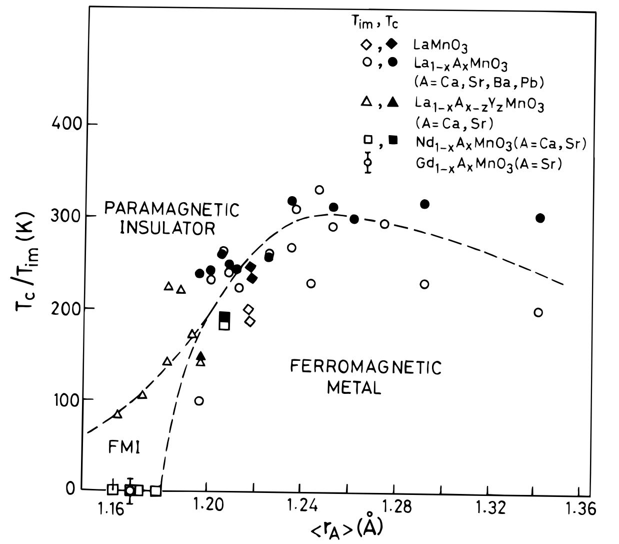

Figure 13. Variation of T_c (T_{im}) of $Ln_{1-x}A_xMnO_3$ with the weighted average radius of the A site cations, $\langle r_A \rangle$ (after ref 27).

(vii) The effect of dimensionality on the MR and other properties of manganates has been examined by a study of the system $(SrO)(La_{1-x}Sr_xMnO_3)_n$.[49] In this system, the three-dimensional perovskite, $La_{1-x}Sr_xMnO_3$, is the $n = \infty$ member, and $La_{1-x}Sr_{1+x}MnO_4$, with the two-dimensional K_2NiF_4 structure, is the $n = 1$ member. The $n = 1$ member is an insulator and does not show ferromagnetism with a well-defined T_c. The $n = 2$ member, on the other hand, shows a sharp I−M transition, a high ρ_p, and large MR (greater than the three-dimensional perovskite). T_c and T_{im} increase with n in this family. The high MR in the $n = 2$ member is considered to be due to the in-plane antiferromagnetic interaction competing with the double-exchange interaction.

(viii) The effect of particle size on the MR of manganates has been studied.[50,51] Samples with very small particle sizes do not show very sharp ferromagnetic or I−M transitions, but the magnitude of MR is apparently unaffected. It is also pertinent that thinner films exhibit larger MR than thicker ones.[52] These observations suggest that long-range ferromagnetic order is not a prerequisite for observing GMR in manganates. It is therefore not surprising that $La_{0.9}Ca_{0.1}MnO_3$, which is antiferromagnetic, shows MR at low temperatures

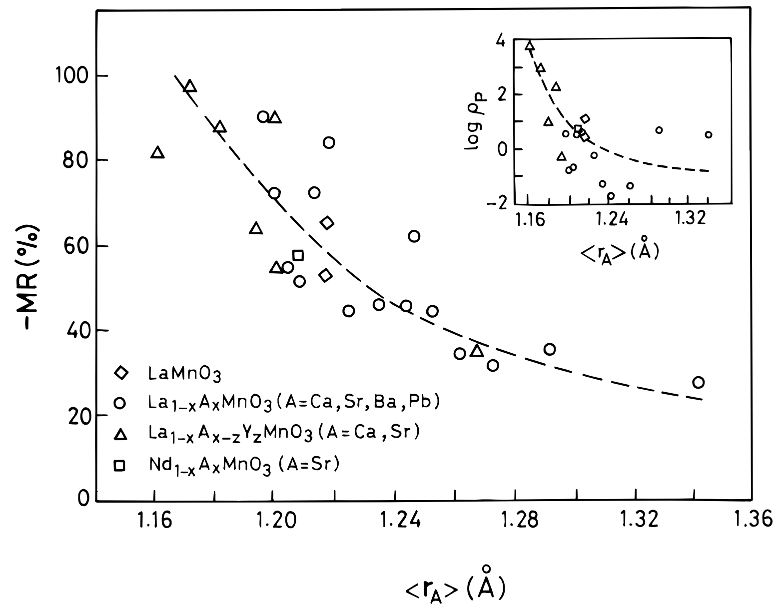

Figure 14. Variation of the magnetoresistance of $Ln_{1-x}A_xMnO_3$ with the weighted average radius of the A site cations, $\langle r_A \rangle$; the inset shows the variation of log ρ_p with $\langle r_A \rangle$ (after ref 27).

(Figure 5) due to the presence of small ferromagnetic Mn^{3+}−O−Mn^{4+} clusters.[43] A study of $La_{0.67}Ca_{0.33}MnO_3$ films prepared by atomic, layer-by-layer molecular beam epitaxy has indeed shown that 15−20 Å superparamagnetic regions are responsible for the GMR.[53] The importance of such superparamagnetism in the GMR of granular metallic films has also been pointed out.[54]

Certain Unusual Features

Some of the properties of the manganates exhibiting GMR are rather uncommon and deserve notice. The first of these pertains to the inhomogeneities that can be present, especially in the samples prepared at low temperatures or without annealing for extended periods at 1270 K or above. On the basis of the variation of the ferromagnetic resonance line width with temperature, the presence of such inhomogeneities has been inferred.[55] The occurrence of broad magnetic and I−M transitions also reflects this feature. The presence of chemical inhomogeneities can be observed directly under favorable circumstances if the ultramicrostructure is examined by high-resolution electron microscopy, although X-ray diffraction patterns may not reveal any evidence for them. The same is true of the intergrowths of related members of a family such as $(SrO)(La_{1-x}Sr_xMnO_3)_n$.

It was mentioned earlier that the T_c and T_{im} of the manganates are generally close to each other. There are instances, however, where the T_{im} is considerably lower than T_c (by 100−200 °C).[56] This happens in samples that are not heated and annealed at high temperatures (>1270 K). What is curious is that widely differing T_{im} values can occur in samples of the same composition (but heat-treated differently), although the magnetic transitions occur sharply at the same temperature. This may be due to differences in the grain sizes. As the annealing temperature is reduced, the grain size decreases, leading to an enhanced contribution from the nonferromagnetic intergrain material; this lowers the susceptibility, makes the material inhomogeneous, and affects ρ and MR.

The most unusual feature of the manganates relates to their electrical resistivity.[15] The resistivity of the manganates at the I−M transition, ρ_p, is rather high, and this high resistivity persists in the "metallic" regime ($T < T_{im}$). The ρ_p values are much higher than Mott's maximum metallic resistivity, which is usually 10^{-2}−10^{-3} Ω cm; typical ρ_p values are >0.05 Ω cm, reaching values up to several thousand Ω cm. The difference between the resistivities at 300 and 4 K is also much larger in the manganates than in the known metallic oxides.[57] In some of the manganates, $\rho(T<T_c)$ is actually larger than $\rho(T>T_c)$. What, then, is this unusual "metallic" state? Coey et al.[58] argue that at $T < T_c$, the e_g electrons are delocalized on an atomic scale, but the spatial fluctuations in the Coulomb and spin-dependent potentials tend to localize the e_g electrons in wavepackets larger than the Mn−Mn distance. A clear description of the nature of metallicity in manganates is difficult at this juncture, although one can attempt to describe it on the basis of comparisons with other oxide systems. Many of the oxides that exhibit compositionally controlled I−M transitions, e.g., $Ln_{1-x}Sr_xCoO_3$, have resistivities comparable to Mott's maximum metallic value at the critical composition.[59] Furthermore, the metallic compositions have a finite density of states at the Fermi level.[60] The $La_{1-x}A_xMnO_3$ system, however, shows a negligible density of states at the Fermi level at ordinary temperatures, even in the "metallic" compositions.[60] They show unusual temperature- and dopant-dependent spectral weight transfer, indicating an unconventional metallic state below T_c, probably polaronic in nature. In Figure 15, we show the valence-band region photoelectron spectra of a few $La_{1-x}Sr_xMnO_3$ compositions to illustrate this important characteristic of the manganates. Oxygen K-absorption spectra show the presence of localized hole states around 1 eV above E_F. Clearly, the metallicity of the manganates differs from that in other oxide systems.

Optical conductivity measurements[61] on $La_{0.825}Sr_{0.175}MnO_3$ as a function of temperature in the 0−10 eV range show a band at 1.5 eV and the spectral weight is

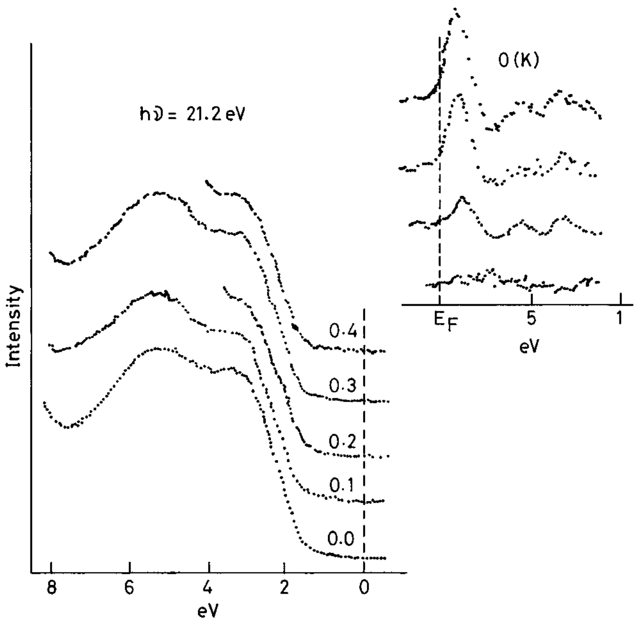

Figure 15. Photoelectron spectra of $La_{1-x}Sr_xMnO_3$ in the valence region at room temperature (from ref 60a).

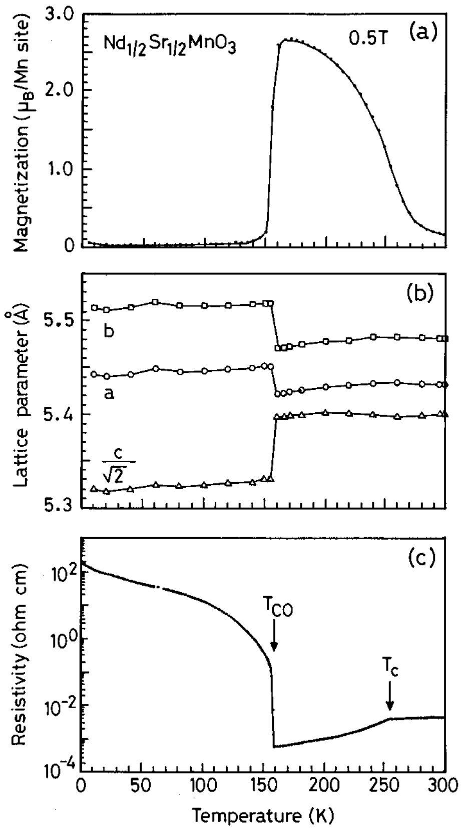

Figure 16. Temperature variation of (a) magnetization, (b) lattice parameters, and (c) resistivity of $Nd_{0.5}Sr_{0.5}MnO_3$ single crystal (from ref 68).

transferred from this band to low energies with decreasing temperature. This band at 1.5 eV is considered to be due to the interband transitions between the exchange-split spin-polarized e_g bands. At $T < T_c$ the conductivity spectrum is dominated by intraband transitions in the e_g band. Recently, an electronic Raman mode has been found at 1800 cm^{-1} in $La_{0.7}Sr_{0.3}MnO_3$; a photoluminescence band is found at 2.2 eV due to intersite electronic transitions of the Mn ions.[62] Both the bands decrease in intensity with increase in temperature. The 1800 cm^{-1} Raman mode could possibly be due to plasmon excitation.

The observation of GMR and related properties in manganates has created considerable interest in the understanding of the properties of these oxides in terms of the electronic structure and theory. The origin of the large magnetoresistance observed near T_c in the manganates is mainly due to the forced alignment of the local t_{2g} spins by the application of a magnetic field causing a reduction in the spin disorder scattering of the e_g electrons.[63] This phenomenon arises from the strong spin-charge coupling (Hund's coupling) between the t_{2g} and e_g electrons[64] on the same Mn atom. This intraatomic ferromagnetic interaction is considerably large compared to the bandwidth and causes a splitting of the e_g band. The double-exchange model essentially explains the behavior of magnetoresistance with respect to magnetization ($-\Delta\rho/\rho = C(M/M_s)^2$).[63] As long as one restricts oneself to relatively wide-band materials such as $La_{1-x}Sr_xMnO_3$, factors such as lattice distortion and disorder seem to be unimportant. However, the situation would be different when the band is narrower as in $La_{1-x}Ca_xMnO_3$. The basic question to understand these manganates is that why they are insulating when $T > T_c$. The anomalous resistance and magnetoresistance has in fact been explained by Millis et al.[65] by considering double exchange along with electron–phonon coupling. The coupling constant varies with temperature and composition. The situation changes from weak coupling to strong coupling leading to a metal–insulator transition. There are however many open questions related to quantum photons, intersite correlations, and so on.

Charge Ordering and Related Effects

The study of GMR and related properties of $Ln_{1-x}A_xMnO_3$ compounds has brought forth novel features related to charge and spin dynamics in these oxides. Charge ordering in metal oxides is not a new phenomenon. Fe_3O_4 (magnetite) undergoes the famous Verwey transition around 120 K due to charge ordering accompanied by a resistivity anomaly, but the ferrimagnetic transition occurs around 860 K. The situation is more interesting in manganates where double exchange gives rise to metallicity along with ferromagnetism, the charge-ordered state being generally associated with insulating and antiferromagnetic (paramagnetic) behavior. The charge-ordered state can be melted into a metallic spin-ordered (ferromagnetic) state, by the application of a magnetic field.

Charge ordering in manganates was first investigated by Jirak et al.[66] by neutron diffraction. An examination of the observations on the rare-earth manganates[67] reveals two types of scenarios, as exemplified by $Nd_{0.5}Sr_{0.5}MnO_3$ and $Pr_{1-x}Ca_xMnO_3$ ($0.3 \leq x \leq 0.5$).[68–70] In the former, a ferromagnetic metallic state ($T_c \sim 250$ K) gives over to an antiferromagnetic charge-ordered state around 150 K (T_{co}) accompanied by changes in lattice parameters as can be seen from Figure 16. $Pr_{0.5}Sr_{0.5}MnO_3$ is similar to $Nd_{0.5}Sr_{0.5}MnO_3$ and shows a transition from a ferromagnetic to an antiferromagnetic state at 140 K.[71] The antiferromagnetic states of $Nd_{0.5}Sr_{0.5}MnO_3$ and $Pr_{0.5}Sr_{0.5}MnO_3$ are of different types (CE and A, respectively); the resistivity anomalies at T_N (T_{co}) are

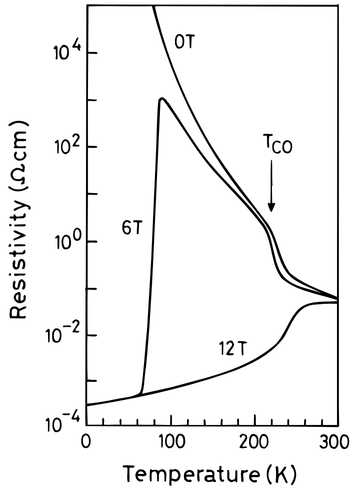

Figure 17. Temperature variation of resistivity under $H = 0$, 6, and 12 T in $Pr_{1-x}Ca_xMnO_3$ ($x = 0.35$) crystal (from ref 70).

also therefore different as suggested by Yoshizawa.[20] The competition between the ferromagnetic double-exchange interaction and the antiferromagnetic charge-ordering instability has been examined in $(Nd,Sm)_{0.5}Sr_{0.5}MnO_3$.[72] In $Pr_{0.7}Ca_{0.3}MnO_3$, an insulating charge-ordered state ($T_{co} \sim 200$ K) becomes antiferromagnetic around 140 K (T_N) and then undergoes a transformation to a canted-spin antiferromagnetic state at a still lower temperature ($T_{CA} \sim 110$ K),[70] as shown in Figure 17. The application of a magnetic field melts the charge-ordered state in all the manganates giving rise to metallic behavior. The first-order insulator−metal (I−M) transition induced by magnetic fields is generally accompanied by considerable hysteresis. This is shown in Figure 18 for $Nd_{0.5}Sr_{0.5}MnO_3$ where the magnitude of hysteresis varies critically with temperature. The I−M transitions in $Nd_{0.5}Sr_{0.5}MnO_3$ and $Pr_{0.5}Sr_{0.5}MnO_3$, where the one-electron bandwidth is controlled by composition, show interesting electronic phase diagrams[67] in the temperature−magnetic field ($T-H$) plane as depicted in Figure 19, where we also show the phase diagram for $Pr_{1-x}Ca_xMnO_3$.

Charge ordering in the manganates is governed by the width of the e_g band which is directly determined by the weighted average radius of the A-site cations, $\langle r_A \rangle$, or the tolerance factor, *t*. This is because a distortion of the Mn−O−Mn bond angle affects the transfer interaction of the e_g conduction electrons (holes). We can describe the spin and charge-ordering phenomena in the rare-earth manganate systems in terms of the generalized phase diagram shown in Figure 20. The diagram shows that when $\langle r_A \rangle$ is large (e.g., $La_{1-x}Sr_xMnO_3$), only ferromagnetism and the associated I−M transition are found with no charge ordering. With decreasing $\langle r_A \rangle$, the ferromagnetic charge−liquid state transforms to the antiferromagnetic charge ordered

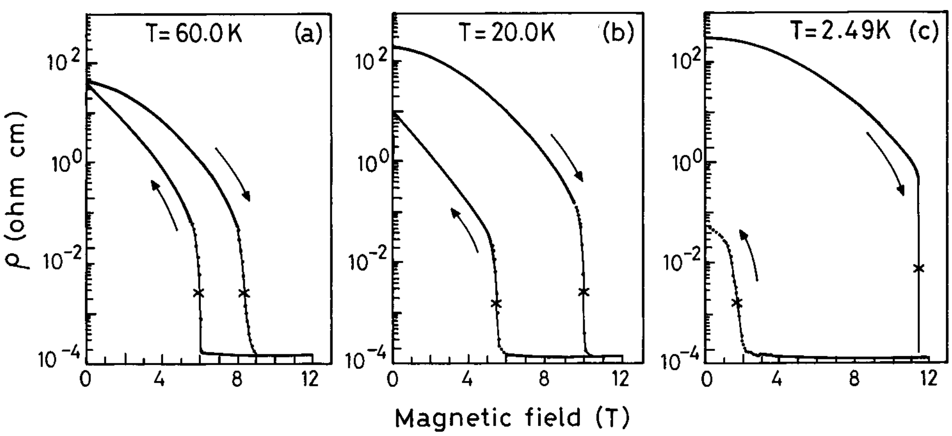

Figure 18. Changes in the resistivity of $Nd_{0.5}Sr_{0.5}MnO_3$ with increasing and decreasing magnetic fields. Notice the sharp jump in resistivity at the lower and upper critical fields (from ref 68).

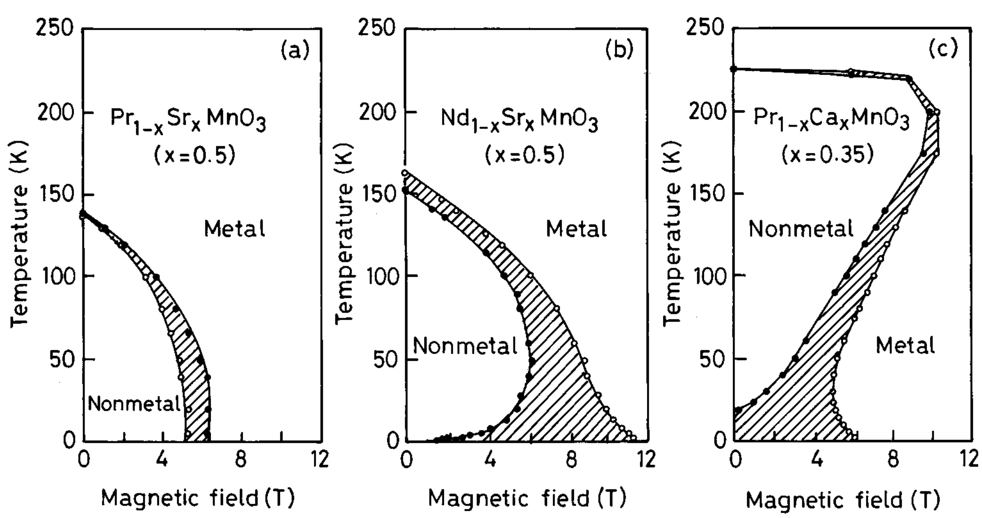

Figure 19. Electronic phase diagrams in the $T-H$ plane of (a) $Pr_{1-x}Sr_xMnO_3$ ($x = 0.5$), (b) $Nd_{1-x}Sr_xMnO_3$ ($x = 0.5$), and (c) $Pr_{1-x}Ca_xMnO_3$ ($x = 0.35$) (from ref 67).

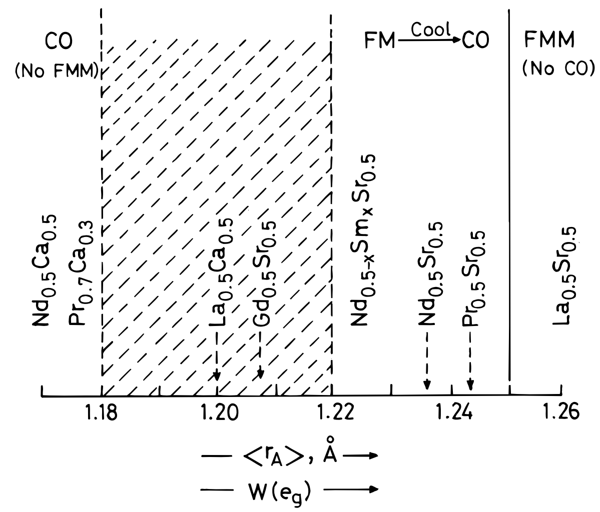

Figure 20. Phase diagram showing the prevalence of charge-ordered (CO) and ferromagnetic states in $Ln_{1-x}A_xMnO_3$ depending on the weighted average radius of the A-site cation, $\langle r_A \rangle$, or the e_g bandwidth.

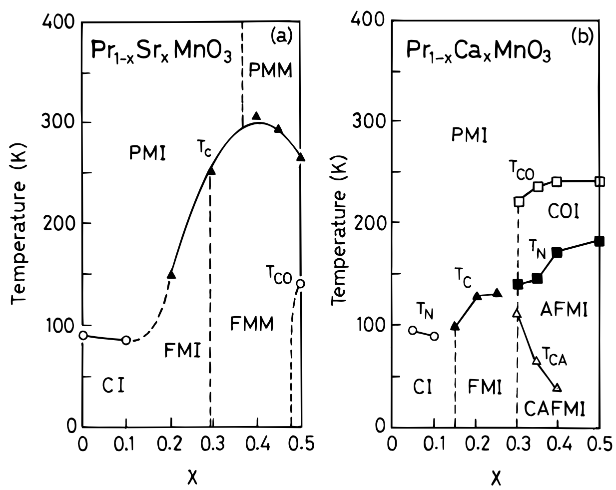

Figure 21. Magnetic and electronic phase diagrams of (a) $Pr_{1-x}Sr_xMnO_3$ and (b) $Pr_{1-x}Ca_xMnO_3$: PMI, paramagnetic insulator; PMM, paramagnetic metal; CSI, canted spin insulator; FMI, ferromagnetic insulator; FMM, ferromagnetic metal; AFMI, antiferromagnetic insulator; CAFMI, canted antiferromagnetic insulator; COI, charge-ordered insulator (from ref 67).

state on cooling (e.g., $Nd_{0.5}Sr_{0.5}MnO_3$). When $\langle r_A \rangle$ is very small as in $Pr_{0.7}Ca_{0.3}MnO_3$ and $Nd_{0.5}Ca_{0.5}MnO_3$, no ferromagnetism occurs, but one finds only a charge-ordered state; the ferromagnetic metallic state is created only by the application of the magnetic field in the charge-ordered state. A recent study[73] of $Nd_{0.5}Ca_{0.5}MnO_3$ shows a first-order transition around 200 K with a large change in volume due to charge ordering; the charge-ordered state can be melted by a magnetic field. It is instructive to compare magnetic and electronic phase diagrams with the generalized phase diagram in Figure 19. We compare the magnetic and electronic phase diagrams of $Pr_{1-x}Sr_xMnO_3$ and $Pr_{1-x}Ca_xMnO_3$ of Tokura et al.[67] in Figure 21.

The $\langle r_A \rangle$ regime between 1.18 and 1.22 Å is interesting and would be expected to show both charge and ferromagnetic ordering. A study of $La_{1-x}Ca_xMnO_3$ in this region has indeed been carried out.[74,75] Charge ordering in these systems is shown by the dramatic increase in sound velocity suggesting the importance of the electron–phonon coupling. At the charge-ordering temperature, these oxides exhibit an anomaly in $d(\ln \rho)/d(T^{-1})$, $\Delta C/T$, and sound velocity[75] as shown in Figure 22. Charge ordering in the 2-dimensional compound $La_{0.5}Sr_{1.5}MnO_4$ has also received attention.[76]

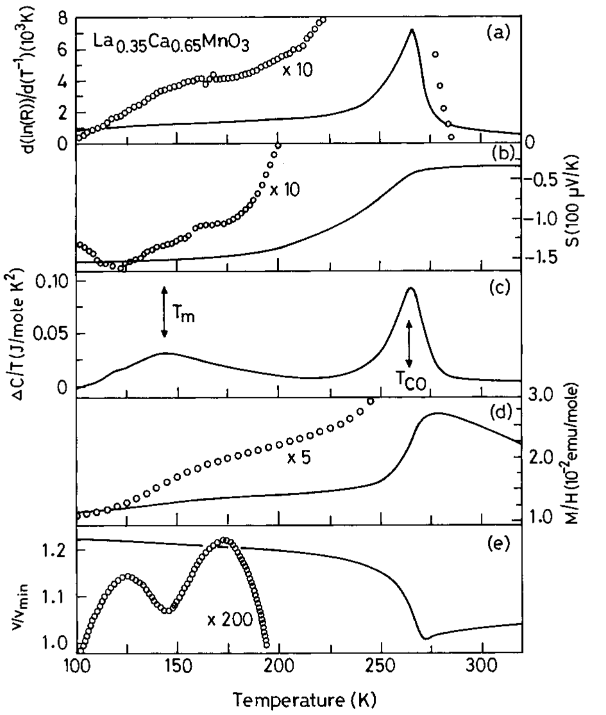

Figure 22. Temperature variation of (a) $d(\ln\rho)/d(T^{-1})$, (b) thermopower, (c) specific heat divided by temperature with lattice estimate subtracted, (d) M/H, and (e) sound velocity of $La_{1-x}Ca_xMnO_3$ ($x = 0.65$). Note the charge ordering transition temperature, $T_{co} = 260$ K (from ref 75).

GMR in Other Oxides

GMR in oxides is not specific to either the perovskites or the manganates. For example, it has been found recently in $Tl_2Mn_2O_7$, which has the pyrochlore structure.[77] The $Ln_{1-x}A_xCoO_3$ family of oxides is also a candidate for GMR, because at a particular value of x the material becomes ferromagnetic and metallic.[59] GMR has been found in some of these cobalt oxides in the insulating regime ($x < 0.1$).[78,79] Magnetoresistance has also been measured in the metallic ferromagnet, $SrRuO_3$.[80]

Concluding Remarks

GMR in manganates has aroused considerable interest in the phenomenon in oxide materials. Although we can explain GMR on the basis of the double exchange model with suitable modifications (e.g., electron–lattice interaction), we are far from understanding the nature of metallicity and the resistivity behavior, specially at low temperatures. Attempts to provide unified models for GMR, charge ordering, and other observations will be attempted, and the increasing variety of good experimental data related to spin, charge and orbital ordering based on neutron scattering and other studies[20] will be of great value in this context.

The common features of GMR in the manganates provide certain guidelines for the discovery or design of new materials. It would be interesting to study quaternary oxides, such as $Ln_{1-x}A_xMn_{1-y}Co_yO_3$, oxide spinels, the $A_2Mn_3O_8$ family of oxides, as well as other oxide systems. The ferromagnetic $LaMn_{1-x}Cr_xO_3$ system would provide a means of delineating exchange from double-exchange interaction. Besides exploring newer materials, there is considerable scope for detailed structural and characterization studies, and physical measurements, on well-characterized manganate materials. The discovery of novel phenomena, such as charge-ordering and field-induced, first-order I−M transitions, portends that new physics and chemistry will emerge from studies of GMR materials. Of particular interest would be studies of valence ordering in manganates by resonant X-ray diffraction[81] and neutron studies of the phase transitions in the presence of a magnetic field. Curiously, there is not sufficient structural information on the manganates around T_c.

References

(1) Baibich, M. N.; Broto, J. M.; Fert, A.; Nguyen Van Dau, F.; Petroff, F.; Etienne, P.; Creuzet, G.; Friederich, A.; Chazeles, J. *Phys. Rev. Lett.* **1988**, *61*, 2472.
(2) Binash, G.; Grünberg, P.; Saurenbach, F.; Zinn, W. *Phys. Rev.* **1989**, *B39*, 4828.
(3) (a) Berkowitz, A. E.; Mitchell, J. R.; Carey, M. J.; Young, A. P.; Zhang, S.; Spada, F. E.; Parker, F. T.; Hatten, A.; Thomas, G. *Phys. Rev. Lett.* **1992**, *68*, 3745. (b) Xiong, P.; Xiao, G.; Wang, J. Q.; Xiao, J. Q., Jiang, J. S., Chien, C. L. *Phys. Rev. Lett.* **1992**, *69*, 3220.
(4) (a) Levy, P. M. *Solid State Phys.* **1994**, *47*, 367. (b) Levy, P. M.; Zhang, S. *J. Magn. Magn. Mater.* **1995**, *151*, 315.
(5) Brandt, N. B.; Moschalkov, V. V. *Adv. Phys.* **1984**, *33*, 193.
(6) (a) von Helmolt, R.; Holzapfel, B.; Schultz, L.; Samwer, K. *Phys. Rev. Lett.* **1993**, *71*, 2331. (b) Chahara, K.; Ohno, T.; Kasai, M.; Kozono, Y. *Appl. Phys. Lett.* **1993**, *63*, 1990.
(7) McCormack, M.; Jin, S.; Tiefel, T.; Fleming, R. M.; Phillips, J. M.; Ramesh, R. *Appl. Phys. Lett.* **1994**, *64*, 3045.
(8) Mahesh, R.; Mahendiran, R.; Raychaudhuri, A. K.; Rao, C. N. R. *J. Solid State Chem.* **1995**, *114*, 297.
(9) Urishibara, A.; Morimoto, Y.; Arima, T.; Asamitsu, A.; Kido, G.; Tokura, Y. *Phys. Rev.* **1995**, *B51*, 14103.
(10) (a) Jonker, G. H.; van Santen, J. H. *Physica* **1950**, *16*, 377. (b) van Santen, J. H.; Jonker, G. H. *Physica* **1950**, *16*, 599.
(11) Zener, C. *Phys. Rev.* **1951**, *82*, 403.
(12) Goodenough, J. B. *Prog. Solid State Chem.* **1971**, *5*, 149.
(13) de Gennes, P. G. *Phys. Rev.* **1960**, *118*, 141.
(14) Wollan, E. O.; Koehler, W. C. *Phys. Rev.* **1955**, *100*, 545.
(15) Mahendiran, R.; Mahesh, R.; Rangavittal, N.; Tewari, S. K.; Raychaudhuri, A. K.; Ramakrishnan, T. V.; Rao, C. N. R. *Phys. Rev.* **1996**, *B53*, 3348.
(16) Schiffer, P.; Ramirez, A. P.; Bao, W.; Cheong, S. W. *Phys. Rev. Lett.* **1995**, *75*, 3336.
(17) (a) van Roosmalen, J. A. M.; Cordfunke, E. H. P.; Helmholdt, R. B.; Zandbergen, H. W. *J. Solid State Chem.* **1994**, *110*, 100. (b) van Roosmalen, J. A. M.; Cordfunke, E. H. P. *J. Solid State Chem.* **1994**, *110*, 109. (c) Hervieu, M.; Mahesh, R.; Rangavittal, N.; Rao, C. N. R. *Eur. J. Solid State Inorg. Chem.* **1995**, *32*, 79.
(18) (a) Mahesh, R.; Kannan, K. R.; Rao, C. N. R. *J. Solid State Chem.* **1995**, *114*, 294. (b) Arulraj, A.; Mahesh, R.; Rao, C. N. R., to be published.
(19) Radaelli, P. G.; Marezio, M.; Hwang, H. Y.; Cheong, S. W. *J. Solid State Chem.* **1996**, *122*, 444.
(20) Abstracts of the JRCAT workshop on spin−charge−lattice coupled phenomena in perovskites, Tsukuba, Japan, May 1996.
(21) (a) Troyanchuk, I. O. *Sov. Phys. JETP* **1992**, *75*, 132. (b) Radaelli, P. G.; Cox, D. E.; Mareio, M.; Cheong, S. W.; Schiffer, P. E.; Ramirez, A. P. *Phys. Rev. Lett.* **1995**, *75*, 4488. (c) Caignaert, V.; Suard, E.; Maignan, A.; Simon, Ch.; Raveau, B. *J. Magn. Magn. Mater.* **1996**, *153*, L260.
(22) Magnetoresistance cannot exceed 100% as defined by eq 1. In the literature, one encounters reports of colossal values of several thousand percent mainly because these workers divide $\Delta\rho$ by $\rho(H)$ instead of $\rho(0)$. Some workers report $100\rho(0)/\rho(H)$ values.
(23) For viable applications, the applied magnetic field has to be small (say 1000 G or less).
(24) While vacancies on either the La or the Mn sites create Mn^{4+} states, a high proportion of Mn vacancies is detrimental to the ferromagnetism and GMR since the d electrons of the MN ions are directly involved in the phenomena.
(25) (a) Raveau, B.; Maignan, A.; Caignaert, V. *J. Solid State Chem.* **1995**, *117*, 424. (b) Caignaert, V.; Maignan, A.; Raveau, B. *Solid State Commun.* **1995**, *95*, 357.
(26) Jia, Y. X.; Lu, L.; Khazeni, K.; Yen, D.; Lee, C. S.; Zettl, A. *Solid State Commun.* **1995**, *94*, 917.
(27) Mahesh, R.; Mahendiran, R.; Raychaudhuri, A. K.; Rao, C. N. R. *J. Solid State Chem.* **1995**, *120*, 204.
(28) Jin, S.; O'Bryan, H. M.; Tiefel, T. H.; McCormack, M.; Rhodes, W. W. *Appl. Phys. Lett.* **1995**, *66*, 180.
(29) Mahendiran, R.; Mahesh, R.; Raychaudhuri, A. K.; Rao, C. N. R. *Phys. Rev.* **1996**, *B53*, 12160.
(30) Mahendiran, R.; Mahesh, R.; Raychaudhuri, A. K.; Rao, C. N. R. *J. Phys. D, Appl. Phys.* **1995**, *28*, 1743.
(31) DeTeresa, J. M.; Blasco, J.; Ibarra, M. R.; Garcia, J.; Marquina, C.; Algarabel, P.; del Moral, A. *Solid State Commun.* **1995**, *96*, 627.
(32) (a) von Helmolt, R.; Wecker, J.; Samwer, K.; Haupt, L.; Barner, K. *J. Appl. Phys.* **1994**, *76*, 6925. (b) Jin, S.; McCormack, M.; Tiefel, T. H.; Ramesh, R. *J. Appl. Phys.* **1994**, *76*, 6929. (c) Ju, H. L.; Kwon, C.; Li, Q.; Greene, R. L.; Venkatesan, T. *Appl. Phys. Lett.* **1994**, *65*, 2108. (d) Lawler, J. F.; Coey, J. M. D. *J. Magn. Magn. Mater.* **1995**, *140−144*, 2049. (e) Gong, G. Q.; Canedy, C.; Xiao, G.; Sun, J. Z.; Gupta, A.; Gallagher, W. *J. Appl. Phys. Lett.* **1995**, *67*, 1783. (f) Hundley, M. F.; et al. *Phys. Rev. Lett.* **1995**, *75*, 860.
(33) Xiong, G. C.; Li, Q.; Ju, H. L.; Mao, S. N.; Senapati, L.; Xi, X. X.; Greene, R. L.; Venkatesan, T. *Appl. Phys. Lett.* **1995**, *66*, 1689.
(34) Sun, J. L.; Krusin-Elbaum, L.; Parkin, S. S. P.; Xiao, G. *Appl. Phys. Lett.* **1995**, *67*, 2720.
(35) Manoharan, S. S.; Vasanthacharya, N. Y.; Hegde, M. S.; Satyalakshmi, K. M.; Prasad, V.; Subramanyam, S. V. *J. Appl. Phys.* **1994**, *76*, 3923.
(36) (a) Gupta, A.; McGuire, T. R.; Duncombe, P. R.; Rupp, M.; Sun, J. Z.; Gallagher, W. J.; Xiao, G. *Appl. Phys. Lett.* **1995**, *67*, 3494. (b) Manoharan, S. S.; Kumar, D.; Hegde, M. S.; Satyalakshmi, K. M.; Prasad, V.; Subramanyam, S. V. *J. Solid State Chem.* **1995**, *117*, 420.
(37) Lawler, J. F.; Lunney, J. G.; Coey, J. M. D. *Appl. Phys. Lett.* **1994**, *65*, 3017.
(38) von Helmolt, R.; Wecker, J.; Lorenz, T.; Samwer, K. *Appl. Phys. Lett.* **1995**, *67*, 2093.
(39) Xiong, G. C.; Li, Q.; Ju, H. L.; Bhagat, S. M.; Lofland, S. E.; Greene, R. L.; Venkatesan, T. *Appl. Phys. Lett.* **1995**, *67*, 3031.
(40) Anane, A.; Dupas, C.; Dang, K. L.; Renard, J. P.; Veillet, P.; Guevara, A. M. D.; Millot, F.; Pinsard, L.; Revcolevschi, A. *J. Phys. Condens. Matter* **1995**, *7*, 7015.
(41) Jia, Y. X.; Lu, L.; Khazemi, K.; Crespi, V. H.; Zettl, A.; Cohen, M. L. *Phys. Rev.* **1995**, *B52*, 147.
(42) Liu, J. Z.; Chang, I. C.; Irons, S.; Klavins, P.; Shelton, R. N.; Song, K.; Wasserman, S. R. *Appl. Phys. Lett.* **1995**, *66*, 3218.
(43) While the T_c, %MR, and other properties vary markedly with $\%Mn^{4+}$, $La_{1-x}A_xMnO_3$ compositions which have a small proportion of Mn^{4+} and are formally antiferromagnetic ($La_{0.9}Ca_{0.1}MnO_3$) still show GMR.
(44) Ju, H. L.; Gopalakrishnan, J.; Peng, J. L.; Li, Q.; Xiong, G. C.; Venkatesan, T.; Greene, R. L. *Phys. Rev.* **1995**, *51*, 6143.
(45) (a) Neumeier, J. J.; Hundley, M. F.; Thompson, J. D.; Heffner, R. H. *Phys. Rev.* **1995**, *B52*, 7006. (b) Moritomo, Y.; Asamitsu, A.; Tokura, Y. *Phys. Rev.* **1995**, *B51*, 16491.
(46) Hwang, H. Y.; Plastra, T. T. M.; Cheong, S. W.; Batlogg, B. *Phys. Rev.* **1995**, *B52*, 15046.
(47) Hwang, H. Y.; Cheong, S. W.; Radadli, P. G.; Marezio, M.; Batlogg, B. *Phys. Rev. Lett.* **1995**, *75*, 914.
(48) Arnold, Z.; Kamenev, K.; Ibarra, M. R.; Algarabel, P. A.; Marquina, C.; Balsco, J.; Garcia, J. *Appl. Phys. Lett.* **1995**, *67*, 2875.
(49) Mahesh, R.; Mahenidran, R.; Raychaudhuri, A. K.; Rao, C. N. R. *J. Solid State Chem.* **1996**, *122*, 448. Moritomo, Y.; Asamitsu, A.; Kuwahara, H.; Tokura, Y. *Nature* **1996**, *380*, 141.
(50) Sanchez, R. D.; Rivas, J.; Vazquez, C. V.; Quintela, A. L.; Causa, M. T.; Tovar, M.; Oseroff, S. *Appl. Phys. Lett.* **1996**, *68*, 134.
(51) Mahesh, R.; Mahendiran, R.; Raychaudhuri, A. K.; Rao, C. N. R. *Appl. Phys. Lett.* **1996**, *68*, 2291.
(52) Jin, S.; Tiefel, T. H.; McCormack, M.; O'Bryan, H. M.; Chen, L. H.; Ramesh, R.; Schurig, D. *Appl. Phys. Lett.* **1995**, *67*, 557.
(53) Rzchowski, M. S.; O'Donnell, J.; Hinaus, B. M.; Onellion, M.; Eckstein, J. N.; Bozovic, I., to be published.
(54) Maeda, A.; Kume, M.; Oikawa, S.; Kuroki, K. *J. Appl. Phys.* **1994**, *76*, 6793.
(55) (a) Lofland, S. E.; Bhagat, S. M.; Ju, H. L.; Xiong, G. C.; Venkatesan, T.; Greene, R. L. *Phys. Rev.* **1995**, *B52*, 15058. (b) Dominguez, M.; Lofland, S. W.; Bhagat, S. M.; Raychaudhuri, A. K.; Ju, H. L.; Venkatesan, T.; Greene, R. L. *Solid State Commun.* **1996**, *97*, 193.
(56) Mahendiran, R.; Mahesh, R.; Raychaudhuri, A. K.; Rao, C. N. R. *Solid State Commun.* **1996**, *99*, 149.
(57) The thermopower, S, shows anomalies[15] around T_c and T_{im}. When x in $La_{1-x}A_xMnO_3$ is small, S is positive and becomes negative at $T > T_{im}$. When $x \approx 0.3$, S becomes more negative at $T < T_{im}$. See also: Asamitsu, A.; Moritomo, Y.; Tokura, Y. *Phys. Rev.* **1996**, *B53*, 2952.

(58) Coey, J. M. D.; Viret, M.; Ranno, L.; Ounadjela, K. *Phys. Rev. Lett.* **1995**, *75*, 3910.
(59) (a) Rao, C. N. R.; Ganguly, P. In *The Metallic and the Nonmetallic States of Matter*; Edwards, P. P., Rao, C. N. R., Eds.; Taylor and Francis: London, 1985. (b) Senaris-Rodriguez, M. A.; Goodenough, J. P. *J. Solid State Chem.* **1995**, *118*, 323.
(60) (a) Sarma, D. D. In *Metal-insulator Transitions Revisited*; Edwards, P. P., Rao, C. N. R., Eds.; Taylor and Francis: London, 1995. (b) Saitoh, T.; Bocquet, A. E.; Mizokawa, T.; Namatame, H.; Fujimori, A.; Abbate, M.; Takeda, Y.; Takano, M. *Phys. Rev.* **1995**, *B51*, 13942. (c) Sarma, D. D.; Shanthi, N.; Kumar, S. R. K.; Saitoh, T.; Mizokawa, T.; Sekiyama, A.; Kobayashi, K.; Fujimori, A.; Wescheke, G.; Meier, R.; Kaindl, G.; Takeda, Y.; Takano, M. *Phys. Rev.* **1996**, *B53*, 6873.
(61) Okimoto, Y.; Katsufuji, T., Ishikawa, T.; Urushibara, A.; Arima, T.; Tokura, Y. *Phys. Rev. Lett.* **1995**, *75*, 109.
(62) Gupta, R.; Sood, A. K.; Mahesh, R.; Rao, C. N. R., to be published.
(63) Furukawa, N. *J. Phys. Soc. Jpn.* **1994**, *63*, 3214.
(64) Inone, J.; Mackawa, S. *Phys. Rev. Lett.* **1995**, *74*, 3407.
(65) Millis, A. J.; Littlewood, P. B.; Shraiman, B. I. *Phys. Rev. Lett.* **1995**, *74*, 5144; *Phys. Rev.* **1996**, *B53*, 8434.
(66) Jirak, Z.; Krupicka, S.; Simsa, Z.; Dlouha, M.; Vratislav, S. *J. Magn. Magn. Mater.* **1985**, *53*, 153.
(67) Tokura, Y.; Tomioka, Y.; Kuwahara, H.; Asamitsu, A.; Moritomo, Y.; Kasai, M. *J. Appl. Phys.* **1996**, *79*, 5288.
(68) Kuwahara, H.; Tomioka, Y.; Asamitsu, A.; Moritomo, Y.; Tokura, Y. *Science* **1995**, *270*, 961.
(69) Lees, M. R.; Barratt, J.; Balakrishnan, G.; McK. Paul, D.; Yethiraj, M. *Phys. Rev.* **1995**, *B52*, 14303.
(70) Tomioka, Y.; Asamitsu, A.; Kuwahara, H.; Moritomo, Y.; Tokura, Y. *Phys. Rev.* **1996**, *B53*, 1689.
(71) Tomioka, Y.; Asamitsu, A.; Moritomo, Y.; Kuwahara, H.; Tokura, Y. *Phys. Rev. Lett.* **1995**, *74*, 5108.
(72) Tokura, Y.; Kuwahara, H.; Moritomo, Y.; Tomioka, Y.; Asamitsu, A. *Phys. Rev. Lett.* **1996**, *76*, 3184.
(73) Vogt, T.; Cheetham, A. K.; Mahendiran, R.; Raychaudhuri, A. K.; Mahesh, R.; Rao, C. N. R., to be published.
(74) Chen, C. H.; Cheong, S. W. *Phys. Rev. Lett.* **1996**, *76*, 4042.
(75) Ramirez, A. P.; Schiffer, P.; Cheong, S. W.; Chen, C. H.; Bao, W.; Palastra, T. T. M.; Gammel, P. L.; Bishop, D. J.; Zegarski, B. *Phys. Rev. Lett.* **1996**, *76*, 3188.
(76) Stemlieb, B. J.; Hill, J. P.; Wildgruber, U. C.; Luke, G. M.; Nachumi, B.; Moritomo, Y.; Tokura, Y. *Phys. Rev. Lett.* **1996**, *76*, 2169.
(77) Shimakawa, Y.; Kubo, Y.; Manako, T. *Nature* **1996**, *379*, 53.
(78) Mahendiran, R.; Raychaudhuri, A. K.; Chainani, A.; Sarma, D. D.; *J. Phys. Condens. Matter* **1995**, *7*, L561.
(79) Briceno, G.; Chang, H.; Sun, X.; Schultz, P. G.; Xiang, X. D. *Science* **1995**, *270*, 273.
(80) Gausepohl, S. C.; Lee, M.; Char, K.; Rao, R. A.; Eom, C. B. *Phys. Rev.* **1995**, *B52*, 3459.
(81) Warner, J. K.; Cheetham, A. K.; Cox, D. E.; Von Dreele, R. B. *J. Am. Chem. Soc.* **1992**, *114*, 6074.

CM960201V